The Journal of Immunology

Mechanisms of Host Defense following Severe Acute Respiratory Syndrome-Coronavirus (SARS-CoV) Pulmonary Infection of Mice

William G. Glass, Kanta Subbarao, Brian Murphy and Philip M. Murphy

References	This article **cites 47 articles**, 12 of which you can access for free at: http://www.jimmunol.org/content/173/6/4030.full#ref-list-1
Subscriptions	Information about subscribing to *The Journal of Immunology* is online at: http://jimmunol.org/subscriptions
Permissions	Submit copyright permission requests at: http://www.aai.org/ji/copyright.html
Email Alerts	Receive free email-alerts when new articles cite this article. Sign up at: http://jimmunol.org/cgi/alerts/etoc

Mechanisms of Host Defense following Severe Acute Respiratory Syndrome-Coronavirus (SARS-CoV) Pulmonary Infection of Mice

William G. Glass,* Kanta Subbarao,[†] Brian Murphy,[†] and Philip M. Murphy[1]*

We describe a model of severe acute respiratory syndrome-coronavirus (SARS-CoV) infection in C57BL/6 mice. A clinical isolate of the virus introduced intranasally replicated transiently to high levels in the lungs of these mice, with a peak on day 3 and clearance by day 9 postinfection. Viral RNA localized to bronchial and bronchiolar epithelium. Expression of mRNA for angiotensin converting enzyme 2, the SARS-CoV receptor, was detected in the lung following infection. The virus induced production in the lung of the proinflammatory chemokines CCL2, CCL3, CCL5, CXCL9, and CXCL10 with differential kinetics. The receptors for these chemokines were also detected. Most impressively, mRNA for CXCR3, the receptor for CXCL9 and CXCL10, was massively up-regulated in the lungs of SARS-CoV-infected mice. Surprisingly Th1 (and Th2) cytokines were not detectable, and there was little local accumulation of leukocytes and no obvious clinical signs of pulmonary dysfunction. Moreover, beige, CD1^{−/−}, and RAG1^{−/−} mice cleared the virus normally. Infection spread to the brain as it was cleared from the lung, again without leukocyte accumulation. Infected mice had a relative failure to thrive, gaining weight significantly more slowly than uninfected mice. These data indicate that C57BL/6 mice support transient nonfatal systemic infection with SARS-CoV in the lung, which is able to disseminate to brain. In this species, proinflammatory chemokines may coordinate a rapid and highly effective innate antiviral response in the lung, but NK cells and adaptive cellular immunity are not required for viral clearance. *The Journal of Immunology,* 2004, 173: 4030–4039.

The causative agent of severe acute respiratory syndrome (SARS)[2] has been identified as a novel coronavirus (CoV), now named SARS-CoV (1–3). CoVs are large positive stranded enveloped RNA viruses that generally cause enteric and respiratory diseases in animals, including humans. The nucleotide sequence of SARS-CoV is highly divergent from those of other CoVs, identifying it as a possible fourth major branch on the CoV phylogenetic tree (1, 4). The difference in sequence is associated with important differences in biology. Most strikingly, whereas other human CoVs cause mild disease with little or no mortality in different groups (5, 6), the human mortality rate following SARS-CoV infection is extremely high, in the range of 10–38% (7, 8). SARS-CoV also uses a unique receptor for cell entry, angiotensin converting enzyme 2 (ACE2), which exists in both membrane-bound and soluble forms (9–12).

Development of antiviral agents specific for SARS-CoV may be facilitated by the development of an animal model of disease. In this regard, the virus has been reported to infect ferrets, domestic cats, and various species of monkeys (13, 14). Moreover, recently Subbarao et al. (15) demonstrated that BALB/c mice could be productively infected with a human clinical isolate of SARS-CoV

although no clinical disease manifestations were identified. These mice clear virus by day 7 postinfection, and develop protective neutralizing Abs by day 28. In this report, we have extended that study in an infection model using C57BL/6 mice (B6). We have switched to B6 mice for two main reasons. First, as a further attempt to develop a mouse model of disease, because BALB/c mice are generally considered to have a Th2 type bias in their immune responses whereas B6 mice are considered to be Th1-biased. This difference could lead to different viral clearance rates and clinical manifestations. Second, to study viral clearance mechanisms, because genetically modified mice are more commonly available on the B6 background. To date, there are limited data on immunopathogenesis in patients with SARS, and these are primarily restricted to serum cytokine levels and circulating blood cell counts. A SARS-CoV model of infection in B6 mice may help identify the determinants of protection and lead to specific treatments and effective vaccine approaches. Our results provide the first detailed immunopathologic and clinical analysis of infection in an animal infected with SARS-CoV and provide evidence for clearance of virus by the innate immune system.

Materials and Methods

Mice

The mouse studies were approved by the National Institute of Allergy and Infectious Diseases (NIAID) Animal Care and Use Committee and were conducted in an approved animal biosafety level 3 facility. All personnel entering the facility wore powered air purifying respirators (HEPA Air-Mate; 3M, Saint Paul, MN). Female C57BL/6 mice (B6), B6.129S7-Rag1^{tm1Mom} (RAG1$^{−/−}$), C.129S2-Cd1$^{tm1Gru/J}$ (CD1$^{−/−}$), and C57BL/6J-Lyst^{bg-J}/J (beige) mice were purchased from The Jackson Laboratory (Bar Harbor, ME). Experiments were initiated when mice were 5–6 wk of age and were performed according to NIAID Animal Care and Use Committee guidelines.

Virus and cells

The Urbani strain, a clinical isolate of SARS-CoV, was passaged twice in Vero E6 cells at the Centers for Disease Control and kindly provided to us by Drs. L. J. Andebon and T. G. Ksiazek (Atlanta, GA). We then passaged the virus two additional times in Vero cells generating a virus stock with a titer of 2.2×10^5 50% tissue culture infective doses (TCID$_{50}$)/ml, which was kept in culture medium at $-70°C$ until use (15, 16). The Vero cells were maintained in OptiPro SFM (Invitrogen Life Technologies, Carlsbad, CA) supplemented with 4 mM L-glutamine. For viral infections, 50 μl of 1×10^4 TCID$_{50}$ SARS-CoV were administered dropwise into the nose of mildly sedated C57BL/6 mice. Mice were monitored visually and weighed daily. Mice were sacrificed via cervical dislocation and organs (lung, brain, spleen, liver, and kidney) were aseptically removed and placed directly in 1 ml of Opti PRO SFM in a 15-ml tube. Tissues were homogenized to completion using an Omni 115v TH homogenizer with disposable 7-mm probes (Omni International, Warrenton, VA). Homogenized tissues were then centrifuged in a tabletop centrifuge at $1500 \times g$ for 25 min. The supernatant was then aliquoted and frozen at $-80°C$ for later use. Viral titers were determined from the supernatants on Vero cell monolayers in 24- and 96-well plates and expressed as TCID$_{50}$ per gram of tissue.

Cytokine measurements

Tissue homogenates were used to determine cytokine and chemokine protein expression using murine Quantikine Immunoassay kits (R&D Systems, Minneapolis, MN) following the manufacturer's directions. All ELISA samples were run in duplicate. For RT-PCR, total RNA was isolated from whole lung, spleen, kidney, brain, heart, and one lobe of the liver using TRIzol (Invitrogen Life Technologies) reagent according to the manufacturer's specifications. To detect SARS-CoV RNA, 2 μg of total RNA was amplified with a TITANIUM One-Step RT-PCR kit (BD Biosciences, San Diego, CA) using random primers (3 μg/reaction) for the first strand synthesis (Invitrogen Life Technologies). The SARS-CoV-specific primers amplify a 310-bp sequence of the polymerase gene [SARS-CoV forward (5'-caccgtttctacaggttagctaacga-3'), SARS-CoV reverse (5'-aaat gtttacgcaggtaagcgtaaaa-3')]. The PCR portion of the one-step process was allowed to run for 35 cycles and analyzed on a 2% Tris-borate-EDTA agarose gel. β_2 Microglobulin primers were used in separate reactions as RNA quantity and PCR controls [β_2 forward (5'-atgggaagccgaacatactg-3'), β_2 reverse (5'-cagtctcagtgggggtgaat-3')]. The PCR portion of this one-step reaction was allowed to run for a total of 30 cycles.

For chemokine, chemokine receptor, and ACE2 (murine ACE2 (mACE2)) gene expression, 2 ng of total RNA were first converted to cDNA using a Superscript III RT kit (Invitrogen Life Technologies), again using random primers and following the manufacturer's specifications. PCR was performed using 2 μl of cDNA in a reaction mix with *Taq* polymerase (Invitrogen Life Technologies). PCR for all chemokines/cytokines and chemokine receptors was run for 30 cycles. The following primers were used: mACE2 forward (5'-ctacaggcccttcagcaaag-3'), mACE2 reverse (5'-tgcccagagcctagagttgt-3'); CCL1 forward (5'-ggatgttgacagcaagagca-3'), CCL1 reverse (5'-tagttgaggcgcagctttct-3'); CCL2 forward (5'-aggtccctgtcatgcttct gbp3'), CCL2 reverse (5'-tctggacccattccttcttg-3'); CCL3 forward (5'-cctctgtcac ctgctcaaca-3'), CCL3 reverse (5'-gatgaattggcgtggaatct-3'); CCL5 forward (5'-gtgcccacgtcaaggagtat-3'), CCL5 reverse (5'-gggaagcgtatacaggtca-3'); CCL7 forward (5'-tgaaaaccccaactccaaag-3'), CCL7 reverse (5'-cattccttaggcgtgaccat 3'); XCL1 forward (5'-cagggccagtaccagaaaga-3'), XCL1 reverse (5'-caatgggtttgggaactgag-3'); CXCL1 forward (5'-gctgggattcacctcaagaa-3'), CXCL1 reverse (5'-tctccgttacttggggacac-3'); CXCL9 forward (5'-aaaatt tcatcacgcccttg-3'), CXCL9 reverse (5'-tctccagcttggtgaggtct-3'); CXCL10 forward (5'-ggatggctgtcctagctctg-3'), CXCL10 reverse (5'-ataaccccttgg gaagatgg-3'); CCR1 forward (5'-gttgggaccttgaaccttg-3'), CCR1 reverse (5'-cccaaaggctcttacagcag-3'); CCR2 forward (5'-agagagctgcagc aaaaagg-3'), CCR2 reverse (5'-ggaaagaggcagttgcaaag-3'); CCR3 forward (5'-tttcctgcagtcctcgctat-3'), CCR3 reverse (5'-ataagacggatggccttgtg-3'); CCR4 forward (5'-gctcctcttacacgcagtcc-3'), CCR4 reverse (5'-cttgccatggtcttggtttt-3'); CCR5 forward (5'-cgaaaacacatggtcaaacg-3'), CCR5 reverse (5'-ttcctactcccaagctgcat-3'); CCR7 forward (5'-gtgtgcttct gccaagatga-3'), CCR7 reverse (5'-ccacgaagcagatgacagaa-3'); CXCR3 forward (5'-tgctagatgcctcggacttt-3'), CXCR3 reverse (5'-cgctgactcagtagcacagc-3'); CX3CR1 forward (5'-ggagactggagccaacagag-3'), CX3CR1 reverse (5'-tcttgtctggctgtgtcctg-3'). Digital images of bands separated on ethidium bromide-stained agarose gels were quantitated using NIH image 1.61 software. The intensity of the chemokine or chemokine receptor primer product was divided by the intensity of the β_2 microglobulin primer product to obtain "normalized units".

In situ hybridization

Lungs and brains were aseptically removed from mice following cervical dislocation and placed directly into 10% normal buffered formalin (Fisher Chemicals, Fairlawn, NJ) for 24 h. Samples were then placed in 70% ethanol and shipped to American Histolabs (Rockville, MD) for paraffin embedding and preparation of 6-μm thick sections. RNase protection was used at all stages and slides were baked at 60°C for 1 h following sectioning. In situ hybridization was performed at Lofstrand Labs (Gaithersburg, MD) using a digoxigenin-labeled probe directed against the SARS-CoV polymerase gene. The probe was generated by amplifying the same 310-bp portion of the SARS-CoV polymerase gene used for PCR, which spans $\sim$75% of the open reading frame. The amplicon was cloned into pCRII-TOPO plasmid (Invitrogen Life Technologies).

Immunohistochemistry

Paraffin embedded tissue sections were stained for CXCL10 expression using a mAb to mouse CXCL10 (PeproTech, Rocky Hill, NJ). Staining was performed by Spring Biosciences (Fremont, CA).

Statistical analysis

For RT-PCR, ELISA and viral titer experiments, statistical significance of differences in the data between groups of mice was evaluated using a two-tailed, two sample unequal variance Student's *t* test. Values of $p \leq 0.05$ were considered to be statistically significant.

Results

C57BL/6 mice replicate SARS-CoV in the lung following intranasal inoculation

To determine whether SARS-CoV can replicate in B6 mice we inoculated the mice with 1×10^4 TCID$_{50}$ U of virus intranasally in a volume of 50 μl, an inoculum previously found to be infectious in BALB/c mice (15). The maximum possible concentration of the initial inoculum in the lung, assuming complete inhalation and equal distribution to both lungs, is $\sim$1 $\times 10^5$ TCID$_{50}$/gm of tissue (lung weight was measured for each mouse). Compared with this calculated benchmark, viral titers in the lung consistently and rapidly increased, peaking at 100-fold greater than the benchmark by day 3 postinfection (Fig. 1). The mice were able to clear virus by day 9 as determined by cytopathic effect (CPE) assay. Consistent with these results, RT-PCR analysis demonstrated that mRNA for mACE2, the cellular receptor for SARS-CoV, was detectable constitutively in the lungs of B6 mice at very low levels (data not shown). To determine where in the lung the virus was replicating, in situ hybridization was performed using a probe directed against the SARS-CoV polymerase gene. SARS-CoV RNA was found in a highly restricted and patchy distribution, localized predominantly in the epithelial lining of a subset of bronchi and terminal bronchioles (Fig. 2). We did not find evidence of SARS-CoV in the alveoli.
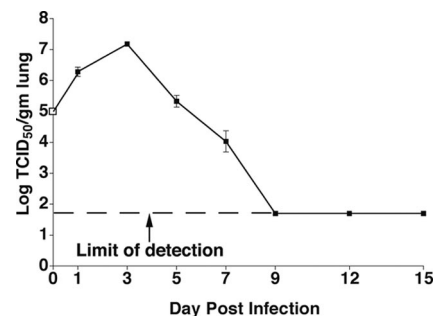

FIGURE 1. SARS-CoV replicates in the lung following intranasal inoculation of B6 mice. Mice were inoculated with 1×10^4 TCID$_{50}$ U of SARS-CoV. Day 0 ($\square$) represents the maximum initial viral burden in the lung calculated by dividing the initial inoculum by lung weight. Data presented are pooled from three separate experiments with a total of 15 mice at each time point, and are presented as the mean $\pm$ SEM.
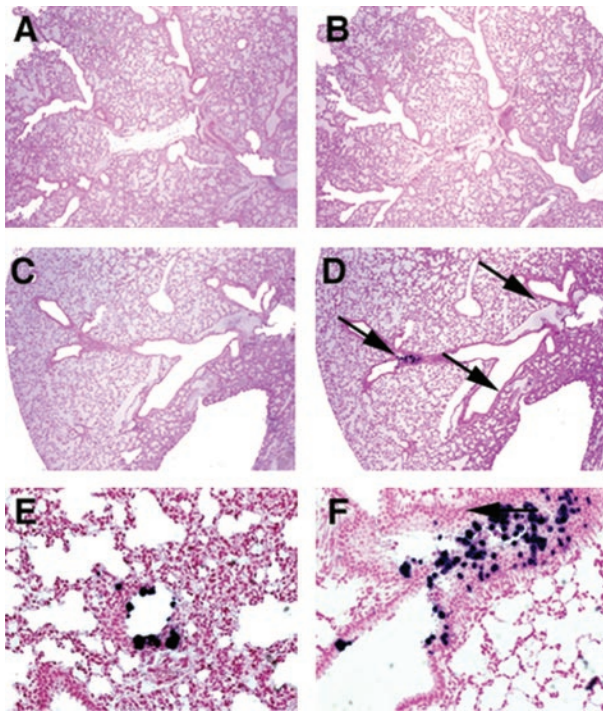
FIGURE 2. SARS-CoV replicates in the terminal bronchioles and bronchi. B6 mice were infected as in Fig. 1. *A–F,* In situ hybridization of SARS-CoV polymerase RNA in mock and SARS-CoV-infected mouse lung. Sense strand (control) probe hybridization is shown in *A,* Mock (×5); *C,* day 3 (×5). Antisense strand probe hybridization is shown in *B,* mock (×5); *D,* day 3 (×10); *E,* day 3 (×20); and *F,* day 3 (×32). The signal in *E* shows virus is localized with terminal bronchiole. The signal in *F* is in a bronchus.

Clearance of SARS-CoV in the mouse does not involve NK cells, NK-T cells, or T and B lymphocytes

NK cells are often an important part of the innate immune response to viral infection. However, beige mice on a B6 background, which selectively lack NK cell function, replicated and cleared virus in the lung with kinetics nearly identical to B6 mice (compare Figs. 1 and 3*A*). To determine what role the adaptive immune response plays in controlling viral infection, we infected CD1$^{-/-}$ mice, which lack NK-T cells, and RAG1$^{-/-}$ mice, which lack T and B lymphocytes, both on a B6 background. SARS-CoV infected and replicated in the lungs of CD1$^{-/-}$ mice with kinetics similar to wild-type B6 mice (Figs. 1 and 3*B*). We attempted several times but were unable to assess viral replication in lungs from RAG1$^{-/-}$ mice by measuring CPE on Vero cells, the only known SARS-

CoV-susceptible cell line that develops CPE. Lung homogenates from uninfected RAG1$^{-/-}$ mice altered the morphology of Vero cells. This was apparently not due to the constitutive presence of IFN-α in the tissue, as suggested by previous reports (17–20), because the effect could not be reproduced by treatment of the cells with recombinant mouse IFN-α at any of a range of concentrations 100-fold above and 100-fold below the IFN-α level we measured in RAG1$^{-/-}$ mouse lung (vide infra). Therefore, other unknown factors in lung homogenates from these mice must account for the background alteration of cell morphology we observed. Given this technical problem, we used two alternative direct methods of determining viral load in these mice. First, we measured virus replication directly in the lung by in situ hybridization with a probe directed against the SARS-CoV polymerase gene. SARS-CoV polymerase was detectable in the lungs of RAG1$^{-/-}$ mice on day 1 postinfection, and increased on day 3, but diminished thereafter and was no longer detectable by day 7. This pattern is nearly identical to that of SARS-CoV-infected B6 mice (Fig. 4*A*). Further, we performed RT-PCR on total RNA isolated from the lungs of both C57BL/6 and RAG1$^{-/-}$ mice infected with SARS-CoV. This also demonstrated increasing viral RNA in the lung to day 3 with a gradual decline to day 9 postinfection (Fig. 4, *B* and *C*). Neither wild-type mice nor any of the three knockout mouse strains tested showed overt signs of clinical disease out to 40 days postinfection.

Induction of inflammatory chemokines in SARS-CoV-infected lung

We next conducted a histopathologic analysis of the lung in SARS-CoV-infected B6 mice. Surprisingly, given the level of viral replication, relatively little leukocyte infiltration was observed, and it was restricted to local inflammatory nodules that colocalized with sites of viral replication, as determined by in situ hybridization. The leukocyte number and differential count in bronchoalveolar lavage fluid from SARS-CoV-infected B6 mice appeared nearly identical to that of mock-infected B6 mice. On day 3 postinfection, the time of greatest viral load, there was evidence of focal necrosis and bronchiolar epithelial damage, characterized by disintegration of bronchiolar lining, granular degeneration of the cells, cell lysis, and pyknosis of nuclei (Fig. 5, *A* and *B*). We also noted mild endothelial swelling (Fig. 5, *C* and *D*). The mild inflammation seen in B6 mice was very similar in RAG1$^{-/-}$ mice (compare Fig. 5*E* with Fig. 5*B*). Interestingly, very little evidence of epithelial damage and/or cellular degeneration was found in SARS-CoV infected RAG1$^{-/-}$ mice, in contrast to infected B6 mice (Fig. 5*F*).

FIGURE 3. NK and NK-T cells are not required for control of SARS-CoV infection. Beige mice (*A*) and CD1$^{-/-}$ mice (*B*) were inoculated intranasally with 1×10^4 TCID$_{50}$ U of SARS-CoV. Day 0 (□) represents the maximum initial viral burden in the lung calculated by dividing the initial inoculum by lung weight. Data are from one experiment with five mice at each time point and are presented as the mean ± SEM.
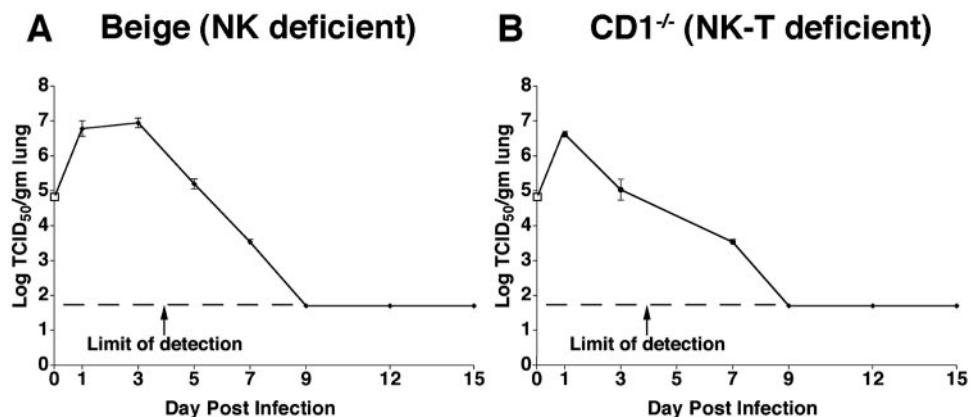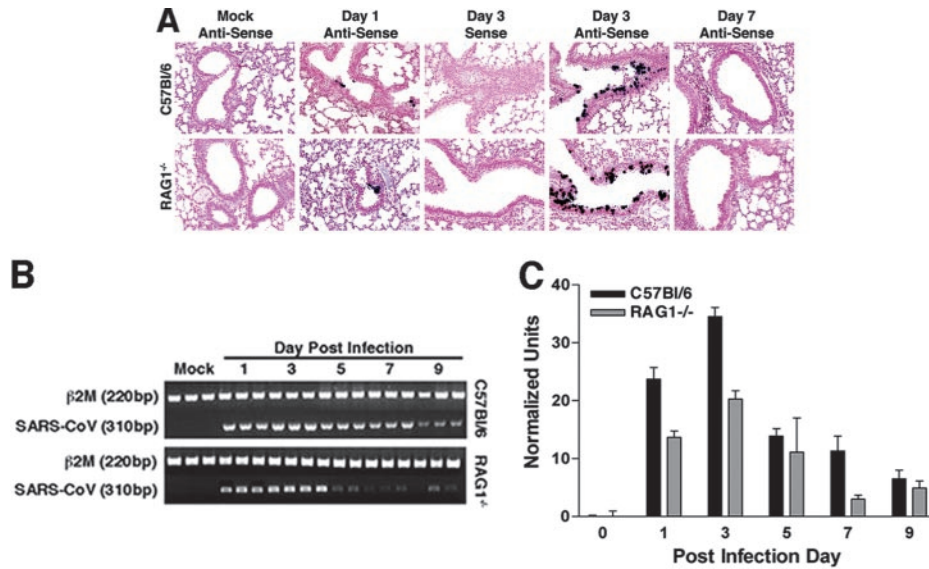
FIGURE 4. SARS-CoV-infected RAG1$^{-/-}$ mice clear virus with the same kinetics as C57BL/6 mice. *A*, In situ hybridization using a probe directed against the SARS-CoV polymerase gene. A sense probe negative control was done for all samples and was negative in each case. Only the day 3 sense control is shown. In both B6 and RAG1$^{-/-}$ lungs, notice the increase in SARS-CoV specific staining until day 3 followed by a rapid decline and absence of staining by day 7. *B*, RT-PCR was performed on RNA isolated from SARS-CoV-infected C57BL/6 and RAG1$^{-/-}$ mice. Each lane represents RNA from an individual mouse (three mice per time point). *C*, Quantitation of RT-PCR products from *B*. $\beta_2M = \beta_2$ microglobulin. Normalized units are defined as the ratio of SARS-CoV PCR product signal intensity to β_2 microglobulin PCR product signal intensity. Data on graph is represented as the mean ± SEM.

To investigate the molecular mechanisms responsible for these changes in the lung, we measured chemokine and cytokine expression. This revealed significantly ($p \leq 0.05$) increased mRNA transcripts for the inflammatory chemokines CCL1, CCL2, CCL3, CCL5, CXCL1, CXCL9, CXCL10, and XCL1 in SARS-CoV-infected C57BL/6 mouse lung compared with mock-infected control mice (Fig. 6*A* and data not shown). CCL4 mRNA was not detected at baseline in the lung and was only minimally induced by SARS-CoV infection. In contrast, CCL7 mRNA was expressed at high levels at baseline in the lung, but was not further increased after infection (data not shown). SARS-CoV infection also induced significant ($p \leq 0.05$) changes in expression levels in the lung for three of the eight chemokine receptors tested, CCR1, CCR3, and CXCR3. Two of these are receptors for four of the up-regulated chemokines: CCR1 for CCL3 and CCL5, and CXCR3 for CXCL9 and CXCL10. CCR1 was constitutively expressed and increased only ~2-fold by viral infection of the lung. In contrast, CXCR3 mRNA was expressed at very low levels in the lungs of uninfected mice but was massively increased by SARS-CoV infection at the same time that its ligands were being induced. CCR3 was constitutively expressed but unlike CCR1 and CXCR3 was strongly down-regulated in the SARS-CoV-infected mouse lung (Fig. 6*B*). Abundant mRNA for the CCL2 receptor CCR2, the CCL3 and CCL5 receptor CCR5, the CCL21 receptor CCR7, and the CX3CL1 receptor CX3CR1 was detected at baseline in the lung but underwent little if any change in amount after infection (data not shown). CCR4 mRNA was expressed at very low levels in lung at baseline and increased only slightly after infection (data not shown).

Chemokines up-regulated by SARS-CoV at the RNA level were also up-regulated at the protein level, as determined by ELISAs performed on lung homogenates (Fig. 7). Kinetic studies of protein expression revealed interesting differential patterns of chemokine expression. For example, CCL2 protein was not detectable in lung from mock-infected B6 mice, but could be detected during a very narrow time window around day 3 after infection, the time of peak viral load. In contrast, CCL3 protein was increased in B6 lungs on
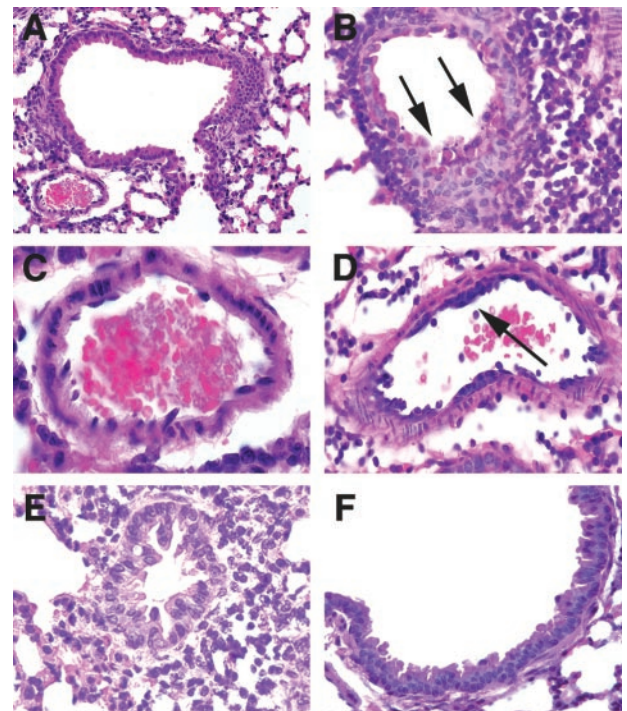

FIGURE 5. Histological changes in the lung epithelium following SARS-CoV infection. *A–F*, H&E-stained sections of C57BL/6 and RAG1$^{-/-}$ mouse lungs. *A*, Mock-infected B6 mouse lung shows normal appearing epithelial lining of a bronchiole (×20). *B*, Day 3 SARS-CoV-infected B6 mouse lung shows granular degeneration of cells (arrows) and mild inflammation (×20). *C*, Mock-infected B6 mouse lung showing normal appearing arterial endothelium (×40). *D*, Day 3 SARS-CoV-infected B6 mouse lung showing arterial endothelial swelling (hypertrophy) and migration of leukocytes (arrow) into lung (×40). *E*, Day 3-infected RAG1$^{-/-}$ mouse lung showing similar inflammation to that of an infected B6 mouse (*B*) (×20). *F*, Day 3-infected RAG1$^{-/-}$ mouse epithelium showing no granular degeneration or rounding of cells as is seen in the lungs of infected B6 mice (*B*) (×20).
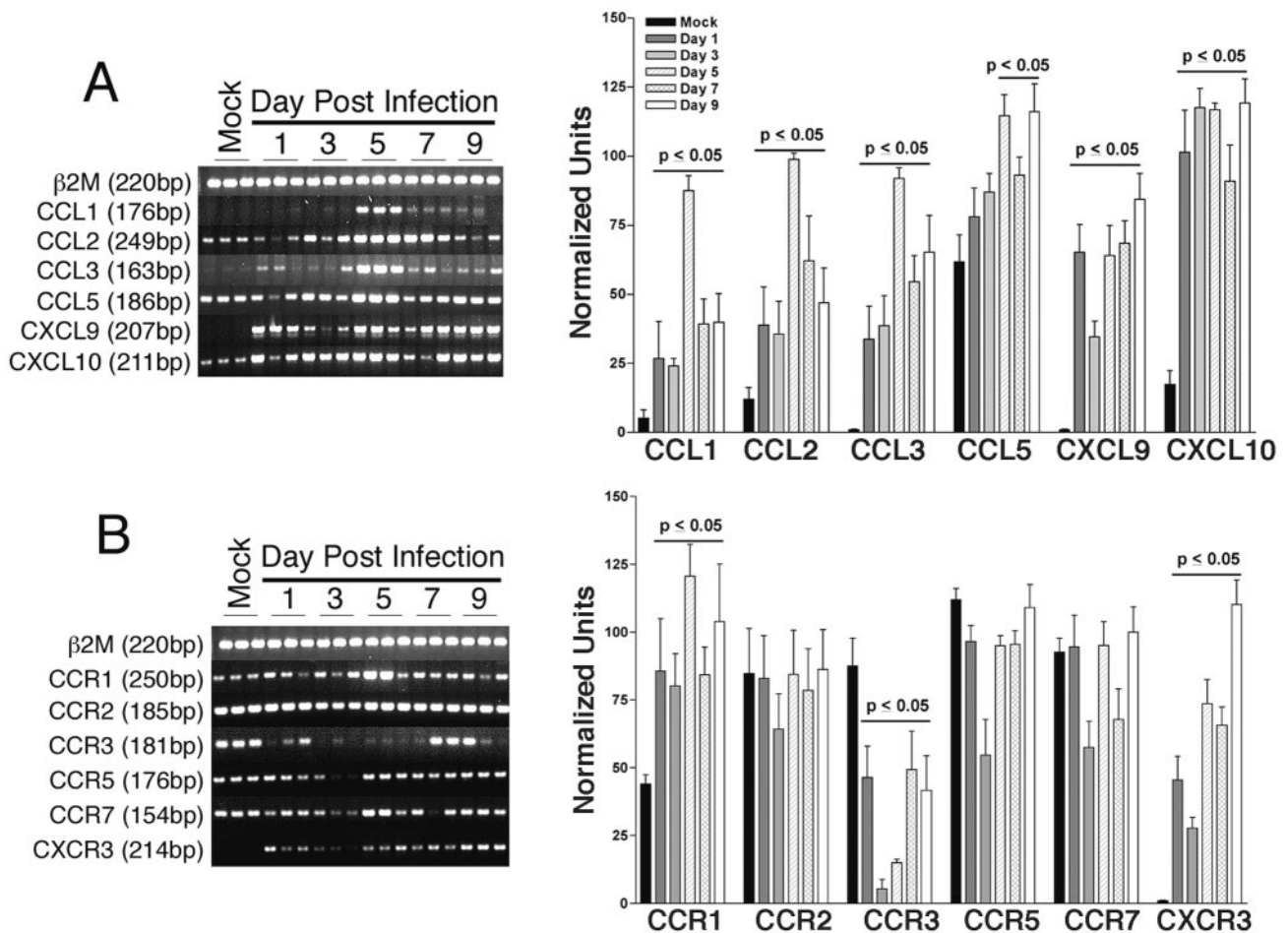
FIGURE 6. SARS-CoV infection induces expression of CC and CXC chemokines and chemokine receptors in C57BL/6 mice. RT-PCR was performed on RNA isolated from mock- and SARS-CoV-infected mice. Quantitation of RT-PCR products is presented in the accompanying graph. *A*, Chemokines; *B*, chemokine receptors; β_2M, β_2 microglobulin. Normalized units are defined as the ratio of SARS-CoV PCR product signal intensity to β_2 microglobulin PCR product signal intensity. Data are pooled from three experiments with eight total mice represented at each time point, and are presented as the mean $\pm$ SEM. Values of *p* are for infected mice at each time point compared with values for mock-infected mice.

day 1 postinfection, peaked on day 3, and persisted to day 9. Lung tissue from mock-infected B6 mice had >4 ng/mg CCL5, and this increased 3-fold by day 7 postinfection. CXCL9 expression was similarly increased in SARS-CoV-infected B6 mice with maximal expression at day 7 postinfection. Although CXCL10 is functionally related to CXCL9 and signals through the same receptor, it was expressed in a distinct pattern in the SARS-CoV-infected B6 lung. Strong early induction of CXCL10 to 11 $\pm$ 1.3 ng/mg was observed on day 3 postinfection, but levels then fell rapidly to the threshold value. Given the dramatic and rapid increase in levels of CXCL10, we used immunohistochemistry to define the lung region and exact cell type producing it. At day 3 postinfection, we found strong immunoreactivity specific for CXCL10 in epithelial cells of terminal bronchioles and upper airways (Fig. 8). Unlike the SARS-CoV distribution revealed by in situ hybridization, CXCL10 immunoreactivity was not patchy and restricted, but instead highly homogeneous in the airway.

SARS-CoV-infected beige and RAG1$^{-/-}$ mice produced a nearly identical pattern of chemokine production as B6 mice although there was a general trend of increased and decreased expression, respectively, in these mice (Fig. 7). Surprisingly, the major primary immunoregulatory cytokines IFN-γ, IL-12 p70, IL-4, IL-10 and TNF-α could not be detected in the lungs of SARS-CoV-infected B6, beige, or RAG1$^{-/-}$ mice at any time point. IFN-α protein was detected at 6.1 $\pm$ 4.4 ng/ml in the lungs of

uninfected RAG1$^{-/-}$ but not B6 or beige mice. However, after infection, expression did not change significantly in RAG1$^{-/-}$ mice and was not induced in B6 or beige.

Failure to thrive following SARS-CoV infection

Although SARS-CoV-infected B6 mice exhibit no overt clinical signs of disease, they gain weight at a reduced rate relative to mock-infected controls, allowing for a measurable disease state (Fig. 9). Nevertheless, there was no mortality in these mice through day 40 postinfection. The mechanism for this relative failure to thrive by SARS-CoV-infected mice was not apparent. Serum levels of aspartate aminotransferase, alanine aminotransferase, lactic dehydrogenase, and blood urea nitrogen were normal (data not shown), suggesting normal liver and kidney function. Further, TNF-α, which is a cachectin, was undetectable in serum throughout the course of the experiment (data not shown). SARS-CoV-infected RAG1$^{-/-}$ mice gained weight normally, which indicates that T and/or B cells may play a role in this phenotype.

SARS-CoV is found in multiple extrapulmonary sites, including the CNS

Despite the fact that SARS-CoV could no longer be cultured from the lung by day 9 postinfection, we were still able to detect viral RNA in the lung by RT-PCR until at least day 15 postinfection (Table I). To determine whether SARS-CoV can spread beyond
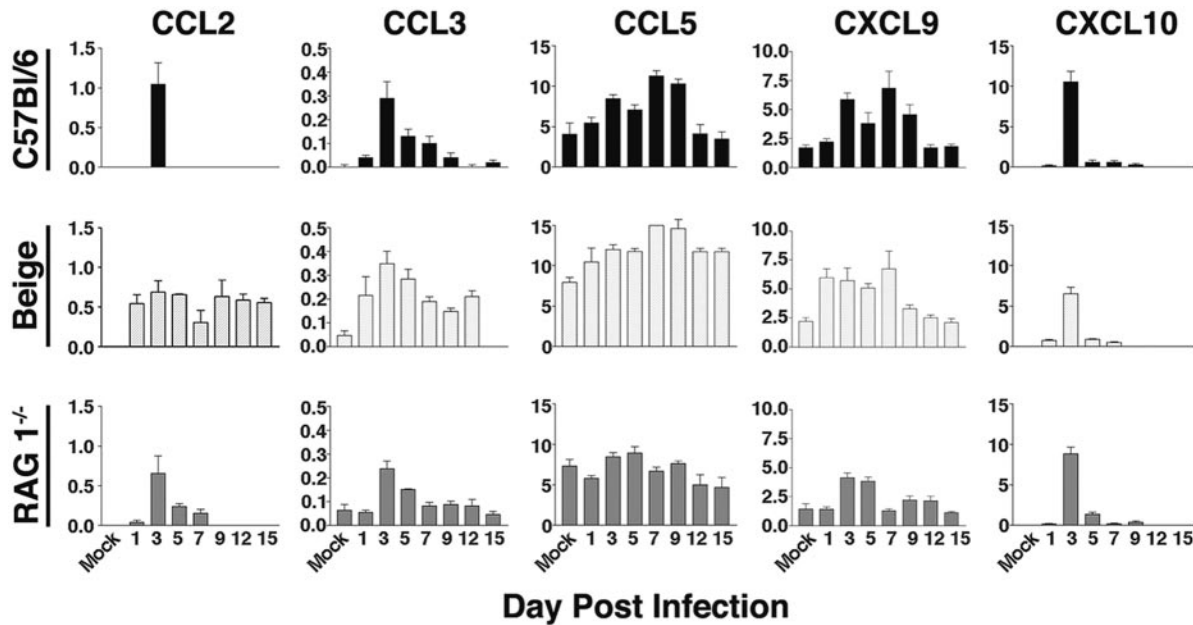
FIGURE 7. Inflammatory chemokines are produced at the protein level in the lung following SARS-CoV infection. All data units are in nanograms per gram of tissue and are presented as the mean ± SEM. The chemokine analyzed is at the top of the corresponding column of graphs; the mouse strain analyzed is at the left of each corresponding row of graphs. Data from C57BL/6 are pooled from three experiments with a total of nine mice at each time point. Data from beige mice are from one experiment with a total of five mice at each time point. Data from RAG1$^{-/-}$ mice are from two experiments with a total of six mice at each time point.

the respiratory tract, multiple extrapulmonary sites were tested by RT-PCR. β_2 microglobulin primers were used as positive controls and revealed roughly equivalent PCR products for all samples. At all days sampled (1, 3, 5, 7, and 9 postinfection) SARS-CoV RNA was detected in the lung, brain, heart, liver and spleen, but not in the kidney, suggesting the virus may spread from the lungs to most other tissues. No PCR product for SARS-CoV was ever found in mock-infected samples (Fig. 10). All of the extrapulmonary sites where RT-PCR evidence of virus was found showed great variability in both signal intensity and frequency of detection, for reasons that are unclear. Extensive microscopic analysis of lung, kidney, spleen, liver, and brain was performed in both mock-infected and SARS-CoV-infected mice out to 40 days postinfection, but only minor histological changes were identified in any of the tissues at any time point following infection.

Brain was the only organ that showed an increase in the number of positive samples with increasing time after infection, which increases the probability that the virus has actually infected this organ instead of simply contaminating it. This prompted us to investigate whether replicating virus could be isolated from this site.

In situ hybridization demonstrated the rare instance of infected cells in the CNS at days 3 and 5 postinfection (one to two cells were found to be infected per 6-μm thick sagittal section of whole brain for each mouse investigated). However, we were unable to isolate live virus from the CNS at these time points. We also investigated the possibility of late infection in the CNS by attempting to isolate live virus from the brain after day 7. We were able to isolate live virus at days 9, 12, and 15 postinfection (Fig. 11). In situ hybridization, which was also performed during this time period, revealed the presence of an ~8-fold increased density of unequivocally positive cells. Interestingly, the virus was predominantly localized to the hippocampus (Fig. 12). As early as day 1 postinfection, IL-12 p70 could be detected in the brain at concentrations >1 ng/mg tissue, and was detected until day 5 postinfection, however IFN-γ and multiple other immunoregulatory cytokines were not detected. Expression of CCL5 protein, which was not detected in samples of mock-infected brain, rose to 890 ± 10 pg/gm brain on day 7 postinfection (Table II). Other chemokines were not detected in mock-infected brain and were not induced by infection with SARS-CoV at any time point tested out to 15 days postinfection.

FIGURE 8. Increased CXCL10 expression in the terminal bronchioles of SARS-CoV-infected mice. Images are lung section of a mock and SARS-CoV-infected mouse stained with a mAb directed against CXCL10, images are ×40.
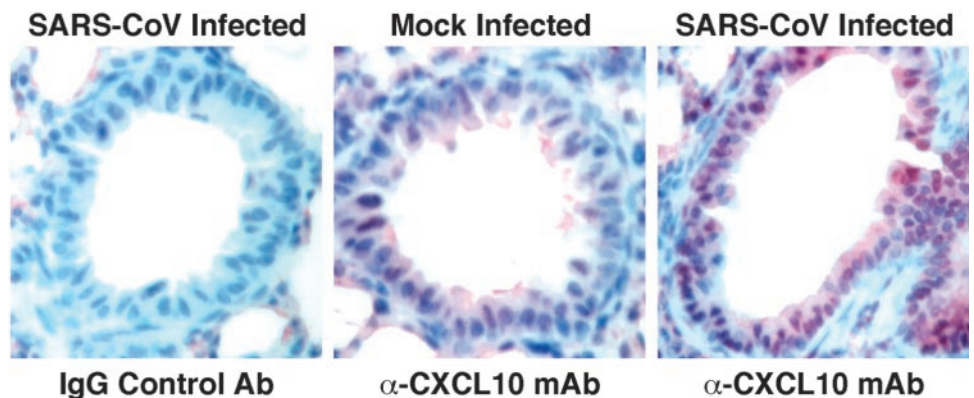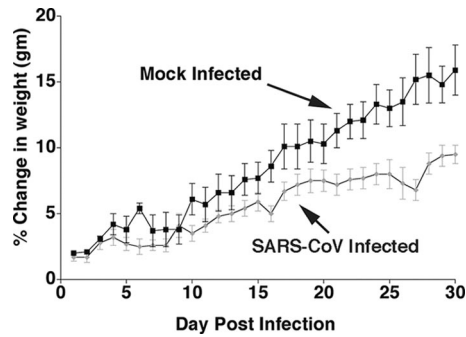
FIGURE 9. C57BL/6 mice fail to thrive following SARS-CoV infection. Percent change in weight from initial weight before infection with 1×10^4 TCID$_{50}$ U of virus was measured on a per mouse basis and averaged for each day. The average starting weight of each group was similar (Mock = 17.5 ± 0.2 gm, SARS-CoV-infected = 17.8 ± 0.1 gm). Data presented are pooled from five experiments with 135 mice at day 1, 120 at day 3, 105 at day 5, 90 at day 7, 75 at day 9, 60 at day 12, 45 at day 15, and 30 at day 30. Data are presented as the mean $\pm$ SEM.

Discussion

This study demonstrates that B6 mice can be productively infected by SARS-CoV in the bronchial and bronchiolar epithelium of the respiratory tract, and that virus is rapidly cleared through a mechanism independent of NK cells, NK-T cells, and T and B lymphocytes. Virus is able to spread to the brain at late time points when it has already been cleared by the lung, and may spread to multiple other organs. SARS-CoV induces dramatic up-regulation of a subset of inflammatory chemokines and the chemokine receptor CXCR3, but interestingly this occurs without detectable expression of classic proinflammatory and immunoregulatory cytokines and without evoking marked leukocyte infiltration of the lung. Overall, infected B6 mice do not develop overt disease, but their weight gain is slowed relative to mock-infected controls.

The work confirms our previously published finding that BALB/c mice can be productively and transiently infected in the terminal bronchioles. The susceptibility of the two strains to SARS-CoV infection and the time course of infection following administration of 1×10^4 TCID$_{50}$ U appear to be similar (15). Our other findings regarding the local tissue response in the lung, viral dissemination, pathology, and clinical manifestations extend the previous work in BALB/c, and provide both the first evidence of a disease phenotype in SARS-CoV-infected mice and the first analysis of the immunologic correlates of viral clearance in the mouse. The results raise new questions for future studies in this species regarding the nature of IFN-γ-independent mechanisms of

Table I. *SARS-CoV is found in multiple extrapulmonary sites*

Day P.I.[a]	Lung[b,c,d]	Kidney	Liver	Spleen	Heart	Brain
0	0/8	0/6	0/6	0/6	0/6	0/8
1	8/8	0/6	6/6	0/6	2/6	2/8
3	8/8	0/6	6/6	5/6	4/6	6/8
5	8/8	0/6	6/6	4/6	4/6	6/8
7	8/8	0/6	6/6	4/6	4/6	8/8
9	8/8	0/6	3/6	1/6	6/6	8/8
12	8/8	ND	ND	ND	ND	ND
15	8/8	ND	ND	ND	ND	ND

[a] P.I. = postinfection.
[b] Data are presented as the number of animals positive for SARS-CoV RNA vs number of animals tested.
[c] Numbers are generated by visualization of SARS-CoV PCR products on an ethidium bromide-stained gel.
[d] Results from all tissues are pooled from two separate experiments.
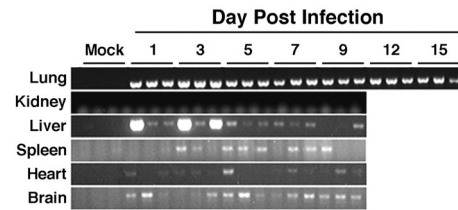

FIGURE 10. SARS-CoV RNA is found in multiple extrapulmonary sites. RNA was extracted from the tissues listed at the indicated days after infection of B6 mice with 1×10^4 TCID$_{50}$ U of SARS-CoV. RT-PCR for the SARS-CoV polymerase gene was performed. Data are presented from one experiment representative of at least two experiments with at least six mice in each group.

IFN-γ-dependent chemokine induction, the mechanism of failure to thrive, the significance of viral dissemination, particularly to the brain, and the innate mechanisms of viral clearance.

With regard to the first main goal of the study, it is clear that the wild-type B6 mouse does not provide a robust model of lethal pulmonary infection with SARS-CoV. However, with regard to the second main goal, our work has succeeded in validating an acute viral infection model for SARS-CoV in B6 mice that could be relevant to subclinical human infection, and in delimiting the range of immunologic control mechanisms. Moreover, these results suggest that it may eventually be possible to develop a pulmonary disease model for SARS in the mouse by experimentally inactivating innate antiviral control systems.

Despite its potential lethality, SARS-CoV usually causes acute resolving infections in humans as it does in B6 and BALB/c mice. However, the exact rate at which humans infected with SARS-CoV clear the virus has not been well-defined. Reports indicate that within the first 2 days of illness, lesions can be found in the lung by chest x-ray, which may increase to day 12 (21). Further, SARS-CoV in the blood of SARS survivors has been reported to drop by approximately one-third at day 7 and by greater than one-half on day 14 of illness (22). Thus, the kinetics of viral replication in the mouse may mimic those in human SARS survivors and humans subclinically infected with SARS-CoV. In this regard, the mouse may provide an adequate small animal model for studies of host defense and other aspects of human infection with SARS-CoV.

Based on our results with beige mice and CD1$^{-/-}$ and RAG1$^{-/-}$ knockout mice, SARS-CoV clearance in the mouse does not require adaptive immunity or NK cell function but appears to rely on innate immune mechanisms. It is important to note however that
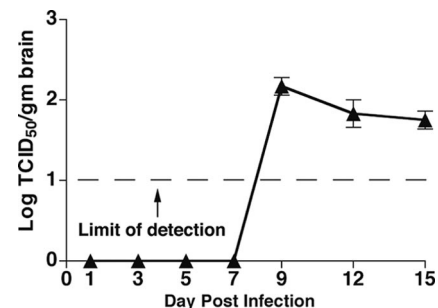
FIGURE 11. SARS-CoV pulmonary infection spread to the CNS, where it is predominantly localized in the hippocampus. B6 mice were inoculated intranasally with 1×10^4 TCID$_{50}$ U of SARS-CoV and brains were removed, homogenized, and clarified homogenate used to determine viral load on Vero cell monolayers in 24-well plates. Data are presented as the mean $\pm$ SEM and are pooled from two separate experiments with a total of six mice at each time point.

Sense

Anti-Sense

FIGURE 12. SARS-CoV pulmonary infection spreads to the CNS, predominantly the hippocampus. Shown at ×10 magnification are serial coronal sections of the hippocampus and surrounding brain harvested 9 days after intranasal infection of a B6 mouse with SARS-CoV. Samples were analyzed by in situ hybridization using probes specific for the SARS-CoV polymerase gene. *B* is a serial section of *A*. Data are representative of three independent experiments.
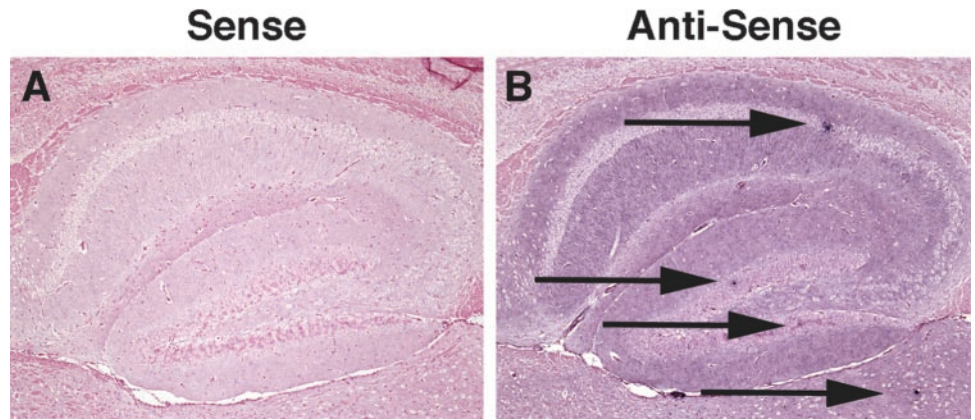
mechanisms to compensate for the loss of B and T lymphocytes or NK cell function could appear during development of these mouse strains, obscuring a role in viral clearance. The lack of a requirement for T or B lymphocytes in initial viral clearance is consistent with the lack of measurable amounts of immunoregulatory cytokines in the lung during infection, and is not unprecedented, but is somewhat surprising in the context of the many viruses that are controlled in whole or in part by the adaptive immune response (23–26). Based on previous work in the BALB/c mouse, SARS-CoV does elicit a humoral immune response, however, it is unlikely to appear early enough to contribute to viral clearance. Determining which component of innate immunity suppresses viral infection in this model is an important question that could provide insight into the pathogenesis and potential treatment and prevention of SARS in human populations. NK cells are clearly not required because beige mice clear virus with kinetics identical to wild type and because there appears to be little if any IFN-α production in the lung during infection. IFN-α only weakly inhibits SARS-CoV infection in vitro even at moderately high doses (27). Moreover, RAG1$^{-/-}$ mice constitutively express high levels of IFN-α in the lung, yet these mice were productively infected with SARS suggesting it does not play an important role in viral clearance. Resident macrophages could be responsible for clearance of SARS-CoV, as they are for parainfluenza-3 virus, Junin virus, and murine poxvirus infection (28–30). Our observation that at the peak of infection only a limited number of cells appeared to be infected in only a subset of airways raises the possibility that mACE-2 and/or other restriction factors are heterogeneously expressed. In this scenario, SARS-CoV infection might be short-

lived because the virus kills all infectable cells quickly, allowing clearance to occur independently of the adaptive immune system.

A striking result of our study was the induction by SARS-CoV in the lung of a subset of inflammatory chemokines (CCL2, CCL3, CCL5, CXCL9, CXCL10) out of proportion to the extent of leukocyte infiltration of the airway. This occurred in infected wild-type B6 as well as beige and RAG1$^{-/-}$ mice and was associated with constitutive and/or induced expression of their cognate receptors CCR1, CCR2, and CXCR3. This is consistent with the report of CCL2 and CXCL10 in the serum of SARS survivors (31). It is also suggestive of a Th1 immune response in these animals. In this regard, the lack of detectable IL-12 p70 or IFN-γ in infected mouse lung is inconsistent and very surprising because expression of both CXCL9 and CXCL10 is tightly controlled by IFN-γ production, to a degree that they are often used as surrogates for it (32). How these chemokines are induced and what role they play in viral clearance remains to be determined. Uncoupling of proinflammatory chemokines from a strong inflammatory infiltrate is likely the reason why overt pneumonia is not seen in these mice. Why the chemokines fail to elicit more of an inflammatory response is not clear. Possible explanations include ineffective temporal and spatial distribution of inflammatory chemokines in the tissue, and expression of chemokine inhibitors, encoded or induced by the virus, that might degrade or scavenge the chemokines as they are produced.

Although adaptive immunity does not appear to be required for clearance of SARS-CoV in this model, this does not mean that an adaptive immune response does not occur. In addition to the specific neutralizing Ab made in response to SARS-CoV infection by

Table II. *Cytokine and chemokine expression in the brains of SARS-CoV-infected C57BL/6 mice*

	Mock[a,b]	Day 1	Day 3	Day 5	Day 7	Day 9	Day 12	Day 15
IFN-α	0	0	0	0	0	0	0	0
IFN-γ	0	0	0	0	0	0	0	0
TNF-α	0	0	0	0	0	0	0	0
IL-4	0	0	0	0	0	0	0	0
IL-10	0	0	0	0	0	0	0	0
IL-12 p70	0	1.2 ± 0.3^{c}	0.14 ± 0.02^{c}	1.3 ± 0.06^{c}	0	0	0	0
CCL2	0	0	0	0	0	0	0	0
CCL3	0	0	0	0	0	0	0	0
CCL5	0	0	0	0	0.13 ± 0.01^{c}	0.15 ± 0.01^{c}	0.89 ± 0.01^{c}	0.10 ± 0.001^{a}
CXCL9	0	0	0	0	0	0	0	0
CXCL10	0	0	0	0	0	0	0	0

[a] Data are presented as nanogram per gram of tissue (mean $\pm$ SEM). Data are pooled from three individual experiments with nine total mice represented.
[b] 0 indicates that expression was below the limits of detection for the assay.
[c] $p \leq 0.01$ when compared to mock-infected mice.

BALB/c mice that was mentioned previously, a Th1 response occurs in response to vaccination of BALB/c mice with SARS-CoV spike protein (15, 33, 34). Data from SARS-CoV-infected human adults show no clear trend toward either a Th1 or Th2 bias. Li et al. (35) show serum increases in IL-2, IL-10, and IL-12. Jones et al. (36) reported decreased IL-2, IL-4, IL-10, and IL-12 producing cells in SARS-CoV-infected patients. Xie et al. (37) have demonstrated a significant increase in TNF-α and IL-8 serum levels. Wong et al. (31) have demonstrated increased IFN-γ, IL-1, IL-6, and IL-12 p70 production, but no IL-2, IL-4, IL-10, or TNF-α, consistent with a Th1 response.

We were able to detect viral genome in the lungs of infected B6 mice by RT-PCR beyond day 9 postinfection, yet at these same time points the virus could not be cultured or demonstrated by in situ hybridization. This could simply reflect the presence of defective or latent virions, neutralized virus or, alternatively, persistent very low level viral infection (38, 39). The latter possibility is interesting in light of our discovery of SARS-CoV in the brain of B6 mice after the lung infection appeared to have cleared. Infection of the brain is consistent with the organotropism of other CoVs, such as HCoV-229E and HCoV-OC43. These and other types of viruses, such as HIV and West Nile virus, often take much longer to become established in the CNS than at the primary site of infection (40, 41). Preferential (but not exclusive) localization of SARS-CoV to the hippocampus in B6 mice is interesting and suggests that studies of memory should be done in these mice. As in the lung, viral infection of the brain was associated with local inflammatory chemokine induction (e.g., CCL5), but the repertoire and temporal pattern were different and no leukocyte infiltration could be detected. Consistent with our results in mice, SARS-CoV has been identified in patient cerebrospinal fluid by quantitative PCR (42), and in brain neurons by immunohistochemistry at autopsy (43). However, to date virus has not been cultured from human CNS specimens. Our data in the mouse and the published human data suggest that SARS-CoV can disseminate to many other organs, including heart, spleen, and liver (44–47). However, these human data must be interpreted with caution because they are based solely on RT-PCR evidence of infection.

In conclusion, our results demonstrate that SARS-CoV is able to infect the bronchial and bronchiolar epithelium of the respiratory tract, spread to the brain, and cause a relative failure to thrive in B6 mice. We have shown that viral clearance does not require NK cells, NK-T cells, or T and B lymphocytes, and we propose that it may involve inflammatory chemokines which are strongly induced by the virus. Work is ongoing to test the precise contribution of specific chemokines to SARS-CoV clearance in the mouse, and to establish a B6 model of SARS pulmonary disease.

References

1. Rota, P. A., M. S. Oberste, S. S. Monroe, W. A. Nix, R. Campagnoli, J. P. Icenogle, S. Penaranda, B. Bankamp, K. Maher, M. H. Chen, et al. 2003. Characterization of a novel coronavirus associated with severe acute respiratory syndrome. *Science* 300:1394.
2. Fouchier, R. A., T. Kuiken, M. Schutten, G. van Amerongen, G. J. van Doornum, B. G. van den Hoogen, M. Peiris, W. Lim, K. Stohr, and A. D. Osterhaus. 2003. Aetiology: Koch's postulates fulfilled for SARS virus. *Nature* 423:240.
3. Drosten, C., S. Gunther, W. Preiser, S. van der Werf, H. R. Brodt, S. Becker, H. Rabenau, M. Panning, L. Kolesnikova, R. A. Fouchier, et al. 2003. Identification of a novel coronavirus in patients with severe acute respiratory syndrome. *N. Engl. J. Med.* 348:1967.
4. Snijder, E. J., P. J. Bredenbeek, J. C. Dobbe, V. Thiel, J. Ziebuhr, L. L. Poon, Y. Guan, M. Rozanov, W. J. Spaan, and A. E. Gorbalenya. 2003. Unique and conserved features of genome and proteome of SARS-coronavirus, an early split-off from the coronavirus group 2 lineage. *J. Mol. Biol.* 331:991.
5. Folz, R. J., and M. A. Elkordy. 1999. Coronavirus pneumonia following autologous bone marrow transplantation for breast cancer. *Chest* 115:901.
6. El-Sahly, H. M., R. L. Atmar, W. P. Glezen, and S. B. Greenberg. 2000. Spectrum of clinical illness in hospitalized patients with "common cold" virus infections. *Clin. Infect. Dis.* 31:96.
7. Manocha, S., K. R. Walley, and J. A. Russell. 2003. Severe acute respiratory distress syndrome (SARS): a critical care perspective. *Crit. Care Med.* 31:2684.
8. Choi, K. W., T. N. Chau, O. Tsang, E. Tso, M. C. Chiu, W. L. Tong, P. O. Lee, T. K. Ng, W. F. Ng, K. C. Lee, et al. 2003. Outcomes and prognostic factors in 267 patients with severe acute respiratory syndrome in Hong Kong. *Ann. Intern. Med.* 139:715.
9. Towler, P., B. Staker, S. G. Prasad, S. Menon, J. Tang, T. Parsons, D. Ryan, M. Fisher, D. Williams, N. A. Dales, et al. 2004. ACE2 x-ray structures reveal a large hinge-bending motion important for inhibitor binding and catalysis. *J. Biol. Chem.* 279:17996.
10. Wang, P., J. Chen, A. Zheng, Y. Nie, X. Shi, W. Wang, G. Wang, M. Luo, H. Liu, L. Tan, et al. 2004. Expression cloning of functional receptor used by SARS coronavirus. *Biochem. Biophys. Res. Commun.* 315:439.
11. Prabakaran, P., X. Xiao, and D. S. Dimitrov. 2004. A model of the ACE2 structure and function as a SARS-CoV receptor. *Biochem. Biophys. Res. Commun.* 314:235.
12. Li, W., M. J. Moore, N. Vasilieva, J. Sui, S. K. Wong, M. A. Berne, M. Somasundaran, J. L. Sullivan, K. Luzuriaga, T. C. Greenough, et al. 2003. Angiotensin-converting enzyme 2 is a functional receptor for the SARS coronavirus. *Nature* 426:450.
13. Haagmans, B. L., T. Kuiken, B. E. Martina, R. A. Fouchier, G. F. Rimmelzwaan, G. Van Amerongen, D. Van Riel, T. De Jong, S. Itamura, K. H. Chan, et al. 2004. Pegylated interferon-α protects type 1 pneumocytes against SARS coronavirus infection in macaques. *Nat. Med.* 10:290.
14. Martina, B. E., B. L. Haagmans, T. Kuiken, R. A. Fouchier, G. F. Rimmelzwaan, G. Van Amerongen, J. S. Peiris, W. Lim, and A. D. Osterhaus. 2003. Virology: SARS virus infection of cats and ferrets. *Nature* 425:915.
15. Subbarao, K., J. McAuliffe, L. Vogel, G. Fahle, S. Fischer, K. Tatti, M. Packard, W. J. Shieh, S. Zaki, and B. Murphy. 2004. Prior infection and passive transfer of neutralizing antibody prevent replication of severe acute respiratory syndrome coronavirus in the respiratory tract of mice. *J. Virol.* 78:3572.
16. Ksiazek, T. G., D. Erdman, C. S. Goldsmith, S. R. Zaki, T. Peret, S. Emery, S. Tong, C. Urbani, J. A. Comer, W. Lim, et al. 2003. A novel coronavirus associated with severe acute respiratory syndrome. *N. Engl. J. Med.* 348:1953.
17. McClane, B. A., A. P. Wnek, and P. Whitaker-Dowling. 1987. Interferon pretreatment enhances the sensitivity of Vero cells to *Clostridium perfringens* type A enterotoxin. *Microb. Pathog.* 3:195.
18. Crespi, M., M. N. Chiu, J. K. Struthers, B. D. Schoub, and S. F. Lyons. 1988. Effect of interferon on Vero cells persistently infected with Sendai virus compared to Vero cells persistently infected with SSPE virus. *Arch. Virol.* 98:235.
19. Kramer, M. J., R. Dennin, C. Kramer, G. Jones, E. Connell, N. Rolon, A. Gruarin, R. Kale, and P. W. Trown. 1983. Cell and virus sensitivity studies with recombinant human α interferons. *J. Interferon Res.* 3:425.
20. Tonew, M., and B. Gluck. 1986. Interferon sensitivity of various cell lines. *J. Basic Microbiol.* 26:173.
21. Li, X. W., R. M. Jiang, J. Z. Guo, and Q. Y. Wang. 2003. Clinical analysis of SARS: 27 cases report. *Zhonghua Yi Xue Za Zhi* 83:910.
22. Hui, D. S., P. C. Wong, and C. Wang. 2003. SARS: clinical features and diagnosis. *Respirology* 8(Suppl.):S20.
23. Grant, M. 2002. Secondary persistent infection with hepatitis C virus: a challenge for adaptive immunity. *Lancet* 359:1452.
24. Mahanty, S., K. Hutchinson, S. Agarwal, M. McRae, P. E. Rollin, and B. Pulendran. 2003. Cutting edge: impairment of dendritic cells and adaptive immunity by Ebola and Lassa viruses. *J. Immunol.* 170:2797.
25. Diamond, M. S. 2003. Evasion of innate and adaptive immunity by flaviviruses. *Immunol. Cell Biol.* 81:196.
26. Siegal, F. P., C. Lopez, P. A. Fitzgerald, K. Shah, P. Baron, I. Z. Leiderman, D. Imperato, and S. Landesman. 1986. Opportunistic infections in acquired immune deficiency syndrome result from synergistic defects of both the natural and adaptive components of cellular immunity. *J. Clin. Invest.* 78:115.
27. Cinatl, J., B. Morgenstern, G. Bauer, P. Chandra, H. Rabenau, and H. W. Doerr. 2003. Treatment of SARS with human interferons. *Lancet* 362:293.
28. Slauson, D. O., J. C. Lay, W. L. Castleman, and N. R. Neilsen. 1987. Alveolar macrophage phagocytic kinetics following pulmonary parainfluenza-3 virus infection. *J. Leukocyte Biol.* 41:412.
29. Contigiani, M. S., S. I. Medeot, G. E. Diaz, and M. S. Sabattini. 1991. Rapid vascular clearance of two strains of Junin virus in *Calomys musculinus*: selective macrophage clearance. *Acta Virol.* 35:144.
30. Karupiah, G., R. M. Buller, N. Van Rooijen, C. J. Duarte, and J. Chen. 1996. Different roles for CD4$^+$ and CD8$^+$ T lymphocytes and macrophage subsets in the control of a generalized virus infection. *J. Virol.* 70:8301.
31. Wong, C. K., C. W. Lam, A. K. Wu, W. K. Ip, N. L. Lee, I. H. Chan, L. C. Lit, D. S. Hui, M. H. Chan, S. S. Chung, and J. J. Sung. 2004. Plasma inflammatory cytokines and chemokines in severe acute respiratory syndrome. *Clin. Exp. Immunol.* 136:95.
32. Gasperini, S., M. Marchi, F. Calzetti, C. Laudanna, L. Vicentini, H. Olsen, M. Murphy, F. Liao, J. Farber, and M. A. Cassatella. 1999. Gene expression and production of the monokine induced by IFN-γ (MIG), IFN-inducible T cell α chemoattractant (I-TAC), and IFN-γ-inducible protein-10 (IP-10) chemokines by human neutrophils. *J. Immunol.* 162:4928.

33. Yang, Z. Y., W. P. Kong, Y. Huang, A. Roberts, B. R. Murphy, K. Subbarao, and G. J. Nabel. 2004. A DNA vaccine induces SARS coronavirus neutralization and protective immunity in mice. *Nature* 428:561.

34. Bisht, H., A. Roberts, L. Vogel, A. Bukreyev, P. L. Collins, B. R. Murphy, K. Subbarao, and B. Moss. 2004. Severe acute respiratory syndrome coronavirus spike protein expressed by attenuated vaccinia virus protectively immunizes mice. *Proc. Natl. Acad. Sci. USA* 101:6641.

35. Li, Z., X. Guo, W. Hao, Y. Wu, Y. Ji, Y. Zhao, F. Liu, and X. Xie. 2003. The relationship between serum interleukins and T-lymphocyte subsets in patients with severe acute respiratory syndrome. *Chin. Med. J. (Engl.).* 116:981.

36. Jones, B. M., E. S. Ma, J. S. Peiris, P. C. Wong, J. C. Ho, B. Lam, K. N. Lai, and K. W. Tsang. 2004. Prolonged disturbances of in vitro cytokine production in patients with severe acute respiratory syndrome (SARS) treated with ribavirin and steroids. *Clin. Exp. Immunol.* 135:467.

37. Xie, J., Y. Han, T. S. Li, Z. F. Qiu, X. J. Ma, H. W. Fan, W. Lu, Z. Y. Liu, Z. Wang, H. L. Wang, and G. H. Deng. 2003. Dynamic changes of plasma cytokine levels in patients with severe acute respiratory syndrome. *Zhonghua Nei Ke Za Zhi* 42:643.

38. Thiel, V., K. A. Ivanov, A. Putics, T. Hertzig, B. Schelle, S. Bayer, B. Weissbrich, E. J. Snijder, H. Rabenau, H. W. Doerr, et al. 2003. Mechanisms and enzymes involved in SARS coronavirus genome expression. *J. Gen. Virol.* 84:2305.

39. Zhang, R., Z. Guo, J. Lu, J. Meng, C. Zhou, X. Zhan, B. Huang, X. Yu, M. Huang, X. Pan, et al. 2003. Inhibiting severe acute respiratory syndrome-associated coronavirus by small interfering RNA. *Chin. Med. J. (Engl.).* 116:1262.

40. Collazos, J. 2003. Opportunistic infections of the CNS in patients with AIDS: diagnosis and management. *CNS Drugs* 17:869.

41. Diamond, M. S., B. Shrestha, A. Marri, D. Mahan, and M. Engle. 2003. B cells and antibody play critical roles in the immediate defense of disseminated infection by West Nile encephalitis virus. *J. Virol.* 77:2578.

42. Hung, E. C., S. S. Chim, P. K. Chan, Y. K. Tong, E. K. Ng, R. W. Chiu, C. B. Leung, J. J. Sung, J. S. Tam, and Y. M. Lo. 2003. Detection of SARS coronavirus RNA in the cerebrospinal fluid of a patient with severe acute respiratory syndrome. *Clin. Chem.* 49:2108.

43. He, L., Y. Q. Ding, X. Y. Che, Q. L. Zhang, Z. X. Huang, H. J. Wang, H. Shen, Z. G. Li, J. J. Cai, J. H. Zhang, et al. 2003. Expression of the monoclonal antibody against nucleocapsid antigen of SARS-associated coronavirus in autopsy tissues from SARS patients. *Di Yi Jun Yi Da Xue Xue Bao* 23:1128.

44. Zhang, Q. L., Y. Q. Ding, J. L. Hou, L. He, Z. X. Huang, H. J. Wang, J. J. Cai, J. H. Zhang, W. L. Zhang, J. Geng, et al. 2003. Detection of severe acute respiratory syndrome (SARS)-associated coronavirus RNA in autopsy tissues with in situ hybridization. *Di Yi Jun Yi Da Xue Xue Bao* 23:1125.

45. Yang, J., Z. H. Wang, J. J. Chen, and J. L. Hou. 2003. Clinical detection of polymerase gene of SARS-associated coronavirus. *Di Yi Jun Yi Da Xue Xue Bao* 23:424.

46. Ren, Y., H. G. Ding, Q. F. Wu, W. J. Chen, D. Chen, Z. Y. Bao, L. Yang, C. H. Zhao, and J. Wang. 2003. Detection of SARS-CoV RNA in stool samples of SARS patients by nest RT-PCR and its clinical value. *Zhongguo Yi Xue Ke Xue Yuan Xue Bao* 25:368.

47. Ding, Y., H. Wang, H. Shen, Z. Li, J. Geng, H. Han, J. Cai, X. Li, W. Kang, D. Weng, et al. 2003. The clinical pathology of severe acute respiratory syndrome (SARS): a report from China. *J. Pathol.* 200:282.